

Metadata of the article that will be visualized in OnlineFirst

ArticleTitle	Synthesis and Characterization of Metal Nanoparticle Embedded Conducting Polymer–Polyoxometalate Composites	
Article Sub-Title		
Article CopyRight - Year	to the authors 2007 (This will be the copyright line in the final PDF)	
Journal Name	Nanoscale Research Letters	
Corresponding Author	Family Name	Viswanathan
	Particle	
	Given Name	Balasubramanian
	Suffix	
	Division	National Centre for Catalysis Research, Department of Chemistry
	Organization	Indian Institute of Technology Madras
	Address	600036, Chennai, India
	Email	bvnathan@iitm.ac.in
Author	Family Name	Kishore
	Particle	
	Given Name	Pilli Satyananda
	Suffix	
	Division	National Centre for Catalysis Research, Department of Chemistry
	Organization	Indian Institute of Technology Madras
	Address	600036, Chennai, India
	Email	
Author	Family Name	Varadarajan
	Particle	
	Given Name	Thirukkallam Kanthadai
	Suffix	
	Division	National Centre for Catalysis Research, Department of Chemistry
	Organization	Indian Institute of Technology Madras
	Address	600036, Chennai, India
	Email	
Schedule	Received	20 August 2007
	Revised	
	Accepted	20 November 2007
Abstract	Phosphomolybdate has been employed simultaneously as the oxidizing agent for the monomer polymerization and the reduced polyoxometalate is used as reducing agent for the reduction of metal ions. The composites thus obtained have been characterized and may have many potential applications.	
Keywords (separated by '-')	Conducting polymer - Polyoxometalates - Organic–inorganic hybrid nanocomposites - Silver - Gold	
Footnote Information		

Journal: NRLT
Article: 11671-9107



Author Query Form

**Please ensure you fill out your response to the queries raised below
and return this form along with your corrections**

Dear Author,

During the preparation of your manuscript for typesetting, some questions have arisen. These are listed below. Please check your typeset proof carefully and mark any corrections in the margin of the proof or compile them as a separate list. This form should then be returned with your marked proof/list of corrections to spr_corrections2@sps.co.in

Disk use

In some instances we may be unable to process the electronic file of your article and/or artwork. In that case we have, for efficiency reasons, proceeded by using the hard copy of your manuscript. If this is the case the reasons are indicated below:

- Disk damaged
- Incompatible file format
- LaTeX file for non-LaTeX journal
- Virus infected
- Discrepancies between electronic file and (peer-reviewed, therefore definitive) hard copy
- Other:

We have proceeded as follows:

- Manuscript scanned
- Manuscript keyed in
- Artwork scanned
- Files only partly used (parts processed differently:))

Bibliography

If discrepancies were noted between the literature list and the text references, the following may apply:

- The references listed below were noted in the text but appear to be missing from your literature list. Please complete the list or remove the references from the text.
- Uncited references*: This section comprises references that occur in the reference list but not in the body of the text. Please position each reference in the text or delete it. Any reference not dealt with will be retained in this section.

Queries and/or remarks

Section/paragraph	Details required	Author's response
References	The reference [37] is given in the list, but not cited in the text. Please check.	

4 Synthesis and Characterization of Metal Nanoparticle Embedded 5 Conducting Polymer–Polyoxometalate Composites

6 Pilli Satyananda Kishore · Balasubramanian Viswanathan ·
7 Thirukkallam Kanthadai Varadarajan

8 Received: 20 August 2007 / Accepted: 20 November 2007
9 © to the authors 2007

10 **Abstract** Phosphomolybdate has been employed simul-
11 taneously as the oxidizing agent for the monomer
12 polymerization and the reduced polyoxometalate is used as
13 reducing agent for the reduction of metal ions. The com-
14 posites thus obtained have been characterized and may
15 have many potential applications.

16
17 **Keywords** Conducting polymer · Polyoxometalates ·
18 Organic–inorganic hybrid nanocomposites · Silver ·
19 Gold
20

21 Introduction

22 The desire to synthesize nanostructures that combine the
23 mechanical flexibility, optical and electrical properties of
24 conducting polymers with the high electrical conductivity
25 and magnetic properties of metal nanoparticles has inspired
26 the development of several techniques for the controlled
27 fabrication of metal nanoparticle–conducting polymer
28 composites. The incorporation of metal nanoparticles into
29 the conducting polymer offers enhanced performance for
30 both the host and the guest [1]. They have diverse applica-
31 tion potentials in electronics because incorporation of metal
32 clusters is known to increase the conductivity of the polymer
33 [2]. The applications of these composites have also been
34 extended to various fields such as, sensors [3, 4], photo-
35 voltaic cells [5], memory devices [6], protective coatings
36 against corrosion [7], and supercapacitors [8]. Of particular

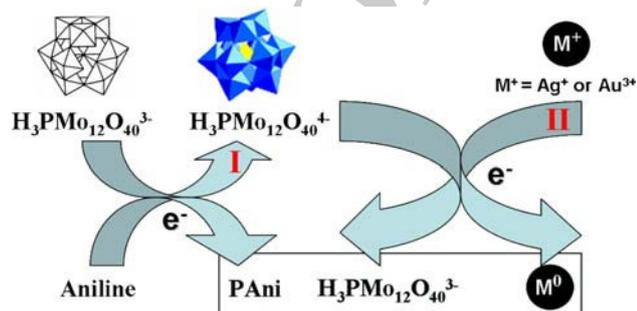
interest is the application of these composites in catalysis. 37
The polymer allows the control of the environment around 38
the metal center, thus influencing selectivity of the chemical 39
reactions. Polyaniline (PAni) supported Pd nanoparticles 40
have been used for the oxidative coupling of the 2,6-di-*t*- 41
butylphenol [9]. In terms of engineering applications, con- 42
ducting polymer-supported metal nanoparticle catalysts are 43
attractive materials for fuel cell design. For example, direct 44
alcohol and proton exchange membrane fuel cell electro- 45
catalysts based on conducting polymers have been studied 46
[10–12]. Dispersing the metal nanoparticles into a con- 47
ducting polymer matrix maintains the electrical connectivity 48
of the particles to the underlying electrode [13, 14]. Under 49
optimal conditions, this arrangement may result in enhanced 50
electrocatalytic properties compared to the corresponding 51
reactivity of the bulk metal [15]. Various methods for the 52
preparation of nanoparticle embedded conducting polymer 53
composites have been described, including template method 54
for growing metal nanoparticles and polymers into nano- 55
structures [16], photochemical preparation [17], and 56
electrochemical methods involving, incorporation of metal 57
nanoparticles during the electrosynthesis of the polymer [18] 58
or electrodeposition of metal nanoparticles on preformed 59
polymer electrodes [19], reduction of metal salts dissolved 60
in a polymer matrix [20], and incorporation of preformed 61
nanoparticles during polymerization of monomers [21] or 62
nanoparticles generated during polymerization [22, 23]. 63
Creation of ideal reaction conditions for the simultaneous 64
reactions (polymerization and nanoparticle formation) is a 65
challenge. The synthesis of nanoparticle and polymer using 66
the same reagent in aqueous solution for generating nano- 67
particles and polymer in the form of a composite is 68
particularly important, as it reduces the number of steps in a 69
complex set of sequential reactions to the formation of a 70
composite. 71

A1 P. S. Kishore · B. Viswanathan (✉) · T. K. Varadarajan
A2 National Centre for Catalysis Research, Department of
A3 Chemistry, Indian Institute of Technology Madras,
A4 Chennai 600036, India
A5 e-mail: bvnathan@iitm.ac.in

72	Polyoxometalates are well-defined metal-oxide poly-	Preparation of Metal Nanoparticles Embedded	119
73	anions that can undergo stepwise and multi-electron reactions	PAni-PMo ₁₂ Composite	120
74	while retaining structural integrity [24]. The introduction of		
75	polyoxometalates into conducting polymer network can be	In a typical experiment, an aqueous solution of PMo ₁₂	121
76	conveniently accomplished by taking advantage of the	(50 mM, 600 μL) was added to aniline monomer (100 μL)	122
77	doping process of polymer leading to incorporation of	and this led to the reduction of PMo ₁₂ and oxidative	123
78	charge-balancing species into the structure [25]. The strong	polymerization of aniline. The appearance of an intense	124
79	oxidizing potential and acidic character of Keggin type	blue color due to the formation of polyoxomolybdate blue	125
80	polyoxometalate, Phosphomolybdic acid (H ₃ PMo ₁₂ O ₄₀ ,	indicated the electron transfer from aniline to PMo ₁₂ .	126
81	PMo ₁₂) provides perfect environment for the polymeriza-	To this solution, 10 mM aqueous solution of AgNO ₃ was	127
82	tion of monomers such as aniline, pyrrole, or thiophene to	added and ultrasonicated for 5 min. This was then allowed	128
83	yield corresponding polymer–polyoxometalate composites.	to stand for 24 h. The as prepared sample (Ag-PAni-	129
84	Different conducting polymers–polyoxometalate compos-	PMo ₁₂) was filtered out, washed, and dried under vacuum.	130
85	ites have been prepared by both chemical and	Similar strategy was adopted for the preparation of Au	131
86	electrochemical routes and used for photoelectrochemical	nanoparticles by using 10 mM HAuCl ₄ to prepare	132
87	and energy storage applications [26–29], but as such, there	Au-PAni-PMo ₁₂ composite.	133
88	are no reports available on the incorporation of metal		
89	nanoparticles on the PAni-PMo ₁₂ composites by using a		
90	single reagent.		
91	The present investigation focuses on the synthesis of Au	Structural Characterization	134
92	or Ag nanoparticles embedded PAni-PMo ₁₂ composites		
93	(Ag-PAni-PMo ₁₂ and Au-PAni-PMo ₁₂) and characteriza-	UV–Visible spectra were recorded on Cary 5E UV–Vis-	135
94	tion of the formed composites. The PMo ₁₂ as reagent for	NIR spectrometer. FTIR investigations were performed	136
95	simultaneous oxidation of aniline and reduction of metal	on Perkin–Elmer 1760 in the region 2,000–400 cm ⁻¹	137
96	salts for the synthesis of nanocomposites has not been	with 32 scans by using KBr pellet mode. Powder X-ray	138
97	reported so far. During the oxidation of aniline, PMo ₁₂ get	diffraction patterns were recorded using a SHIMADZU	139
98	reduced to heteropoly blue which then serve as reducing	XD-D1 diffractometer using a Ni-filtered Cu Kα radiation	140
99	agent for the metal (Ag and Au) ions to form metal	(λ = 1.5418 Å at a 0.2° scan rate (in 2θ)). The morphol-	141
100	nanoparticles. The high-resolution transmission electron	ogy of the composites was investigated by a scanning	142
101	microscopic analysis revealed formation of metal embed-	electron microscopy (SEM) (FEI, Model: Quanta 200).	143
102	ded polymer nanostructures. The present method can also	The transmission electron micrograph (TEM) analysis	144
103	be extended for the preparation of various metal nanopar-	was performed on CM12/STEM working at a 100 kV	145
104	ticles containing nanocomposites with different conducting	accelerating voltage. High-resolution transmission	146
105	polymers such as polypyrrole and poly(3,4-dioxy thio-	electron microscopy (HRTEM) was carried out on a	147
106	phene). Further, the properties of the inorganic–organic	JEOL-3010 instrument operating at 300 kV. Textural	148
107	composites can be tailored by simply varying the polymer	characteristics of composites were determined from	149
108	or polyoxometalate which are desired for electrocatalytic	nitrogen adsorption/desorption at 77 K using a Micro-	150
109	and sensor applications.	metrics ASAP 2020 instrument. The specific surface area,	151
		average pore diameters were determined. Prior to the	152
		measurements, the samples were degassed at 423 K.	153
		The BET specific surface area was calculated by using	154
		the standard Brunauer, Emmett, and Teller method on the	155
110	Experimental	basis of the adsorption data. The pore size distributions	156
111	Materials	were calculated applying the Barrett–Joyner–Halenda	157
		(BJH) method. For conductivity measurements the compos-	158
112	Aniline from Aldrich was distilled under vacuum prior to	posites were pressed in a manual hydraulic press at	159
113	use. Phosphomolybdic acid (H ₃ PMo ₁₂ O ₄₀ , PMo ₁₂) was	750 MPa into a pellet of 13-mm diameter and 0.56-mm	160
114	procured from Aldrich and used further without purifica-	thickness. The conductivity measurements of Au-PAni-	161
115	tion. AgNO ₃ and HAuCl ₄ were obtained from Sisco	PMo ₁₂ and Ag-PAni-PMo ₁₂ were measured by the four-	162
116	research laboratories and used as received. Ultrasonic	point Van der Pauw method [30]. The experimental setup	163
117	treatment of the composites was performed on TOSHCON	included a Keithley 225 current source and Agilent	164
118	sonicator (20 KHz, 100 W), India.	34401 voltmeter.	165

166 Results and Discussion

167 Polyoxometalates can be reduced in a plethora of ways, for
 168 example photochemically [31], through $^{60}\text{Co-}\gamma$ radiolysis
 169 [32], electrolytically [33], and with reductants [34]. The
 170 reduced polyoxometalate has served as reducing agent and
 171 stabilizing agent for the formation of various metal nano-
 172 particle–polyoxometalate composites [35]. Gordeev et al.
 173 have noticed the ability of radiolytically two-electron
 174 reduced 12-tungstophosphate, $[\text{PW}_{12}\text{O}_{40}]^{5-}$, to reduce Ag
 175 ions into stable silver hydrosols [36]. The synthesis of
 176 metal nanoparticle–polyoxometalate composites based
 177 photo-catalytic reduction has been pioneered by Papacon-
 178 stantinou et al. [31]. Wherein, polyoxometalates
 179 ($\text{SiW}_{12}\text{O}_{40}^{4-}$, $\text{PW}_{12}\text{O}_{40}^{3-}$) have served as photocatalysts and
 180 stabilizing agents for the formation of metal nanoparticles.
 181 Recently, Sastry et al. developed the synthesis of Au–Ag
 182 core shell nanoparticles using redox switching ability of
 183 Keggin ions [36]. In the present work, the formation
 184 of reduced PMo_{12} was observed during the polymerization
 185 of aniline in the presence of PMo_{12} . The reduced PMo_{12}
 186 species served as reducing agent for the reduction of metal
 187 ions to form metal nanoparticle embedded PAni-PMo_{12}
 188 composite. The different stages of synthesis of the com-
 189 posites (Steps I and II, Scheme 1) were monitored by UV–
 190 Vis spectra (Fig. 1). Figure 1a corresponds to the UV–Vis
 191 spectrum recorded from PMo_{12} solution which has no
 192 obvious absorbance in the range 400–800 nm. Figure 1b
 193 corresponds to the UV–Vis absorption of the blue-colored
 194 solution containing PMo_{12} and aniline (step I, Scheme 1);
 195 the presence of an absorption band at 700 nm can be seen
 196 and is characteristic of one-electron reduced PMo_{12} (elec-
 197 tron is transferred from aniline to PMo_{12}). The produced d^1
 198 metal ion [38] of Mo is responsible for the d – d transition
 199 resulting in absorption in the visible region. Figure 1c, d
 200 correspond to the spectra of PMo_{12} -PAni solution to which
 201 AgNO_3 and HAuCl_4 solutions were added respectively
 202 (Step II, Scheme 1); strong absorption bands at 450 and
 203 573 nm due to the excitation of surface plasmon resonance



Scheme 1 Schematic representation of the PMo_{12} -mediated synthesis of metal nanoparticle embedded PAni-PMo_{12} composites

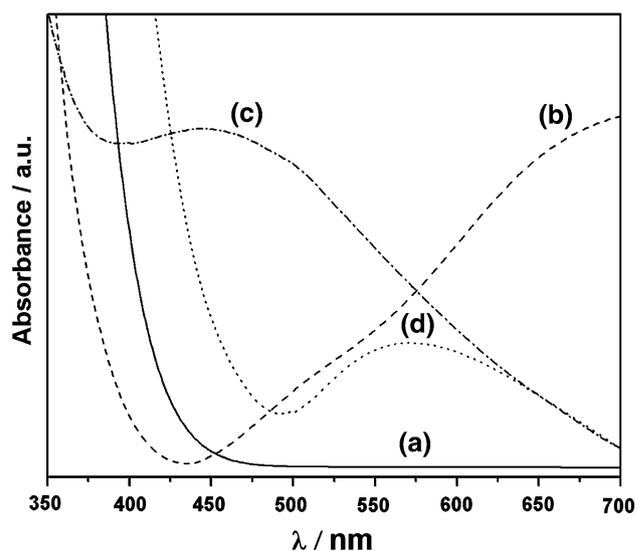


Fig. 1 UV–Vis spectra of (a) 10 mM PMo_{12} (b) a mixture of 5 mM PMo_{12} and 20 μL of aniline (c) after addition of 10 mM AgNO_3 (d) after addition of 10 mM HAuCl_4

on Ag and Au nanoparticle in Ag-PAni-PMo_{12} (Fig. 1c) and Au-PAni-PMo_{12} (Fig. 1d), respectively, were observed.

The presence of Ag and Au nanoparticles in Ag-PAni-PMo_{12} and Au-PAni-PMo_{12} was further confirmed by powder XRD measurements, as shown in Fig. 2. The XRD pattern of Ag nanoparticles containing composite showed four strong peaks with maximum intensity at 38.1° , 44.3° , 64.4° , and 77.4° representing Bragg's reflections from (111), (200), (220), and (311), planes of the standard cubic phase of Ag (Fig. 2a). Au-PAni-PMo_{12} composite also exhibited the presence of four strong peaks with maximum intensity at 38.2° , 44.4° , 64.5° , and 77.5° representing (111), (200), (220), and (311) planes of standard cubic phase of Au (Fig. 2b).

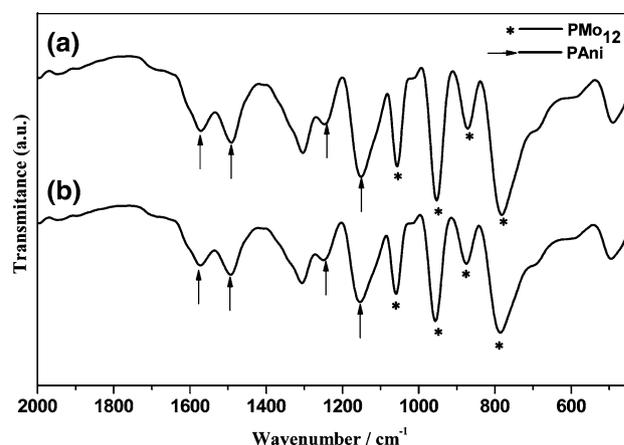


Fig. 2 FTIR spectra of (a) Ag-PANI-PMo_{12} and (b) Au-PANI-PMo_{12}

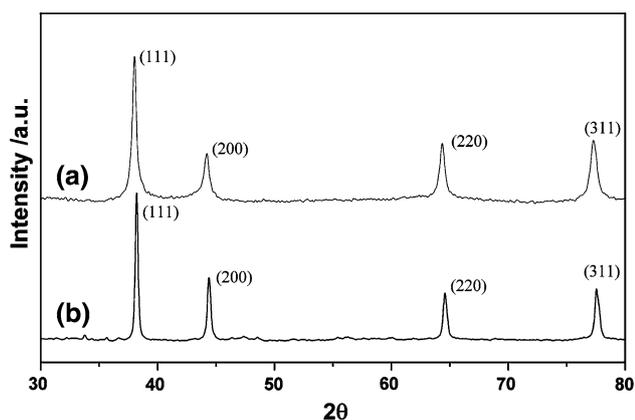


Fig. 3 XRD patterns of (a) Ag-PANI-PMO₁₂ and (b) Au-PANI-PMO₁₂

219 In order to confirm the presence of PANi and the phosphomolybdate anion in the composites, Fourier transform infrared (FTIR) analysis of the Ag-PANI-PMO₁₂ and Au-PANI-PMO₁₂ (Fig. 3a, b) nanocomposites was carried out. Both the composites showed the characteristic bands of PANi (marked with arrows) and phosphomolybdate anion (marked with circles). The peak at 1,575 cm⁻¹ is assigned to a deformation mode of benzene rings, the one at 1,488 cm⁻¹ to a deformation of benzene or quinoide rings, the one at 1,248 and 1,147 cm⁻¹ to a C=N stretching of a secondary amine, at 1,060 cm⁻¹ to a P-O bond, at 955 cm⁻¹ to a Mo=O terminal bond, at 876 cm⁻¹ to a vertex Mo-O-Mo bond, and finally at 800 cm⁻¹ to an edge Mo-O-Mo bond.

233 The nitrogen adsorption/desorption isotherms of Ag-PANI-PMO₁₂ and Au-PANI-PMO₁₂ composites are shown in Fig. 4a, b respectively. The isotherms were identified as type IV isotherms with H3 type Hysteresis

237 loops. The pore size distributions were calculated and represented in the insets of Fig. 4a, b. Both the composites exhibited a broad distribution of mesopores ranging from 2 nm to 43 nm. The average pore sizes were determined and found to be 23.8 nm for Au-PANI-PMO₁₂ and 22.4 nm for Ag-PANI-PMO₁₂. The BET surface areas were also found to be similar, 7 and 6 m²/g for Ag-PANI-PMO₁₂ and Au-PANI-PMO₁₂ composites respectively.

245 The morphology of the prepared nanocomposites was examined using scanning electron microscopy (SEM). Figure 5a, b shows the SEM images of Ag-PANI-PMO₁₂ and Au-PANI-PMO₁₂ composites, respectively. The nanocomposites exhibited a highly mesoporous structure which is of great interest for their application as electrodes since it represents an optimization of the electrode-electrolyte interface.

253 Figure 6a, b shows typical low-magnification TEM images of the Ag-PANI-PMO₁₂ composites. The spherical Ag nanoparticles are well distributed and stabilized by the polymer. The corresponding histogram (Fig. 7a) of the size distribution of the Ag nanoparticles indicates a broad distribution ranging from 3.5 nm to 9 nm of the Ag nanoparticles formed during the reaction. TEM images of Au-PANI-PMO₁₂ composite (Fig. 6c, d) show most of the Au nanoparticles aggregated with a size distribution ranging from 4 nm to 9 nm (Fig. 7b). The particles are aggregated into dendritic structures composed of nanorod arms with an average diameter of ca 3 nm and length 10 nm and they were rather polydisperse. The detailed structure of the Ag and Au nanoparticles in the prepared nanocomposites was further revealed by high-resolution TEM (Fig. 8). From Fig. 8a, it can be seen that the spherical silver nanoparticles embedded in PANi polymer in the Ag-PANI-PMO₁₂ composite and nanoparticles have

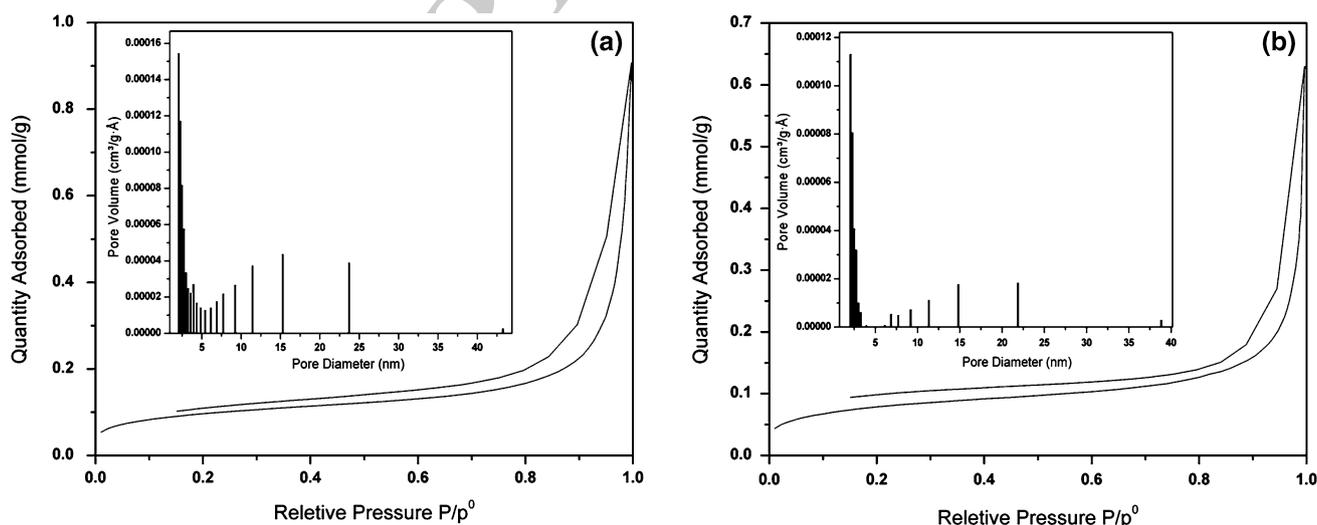


Fig. 4 N₂ adsorption/desorption isotherms of (a) Ag-PANI-PMO₁₂ and (b) Au-PANI-PMO₁₂ (inset: the BJH pore size distribution)

Fig. 5 SEM images of (a) Ag-PANI-PMO₁₂ and (b) Au-PANI-PMO₁₂

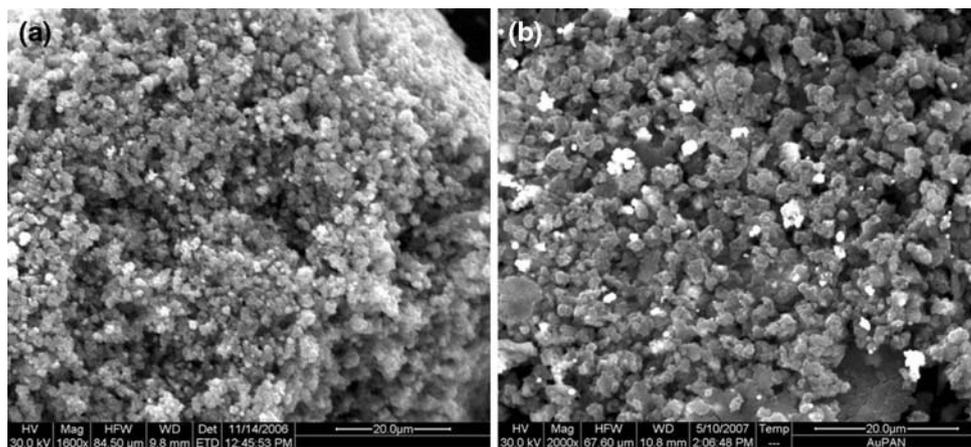
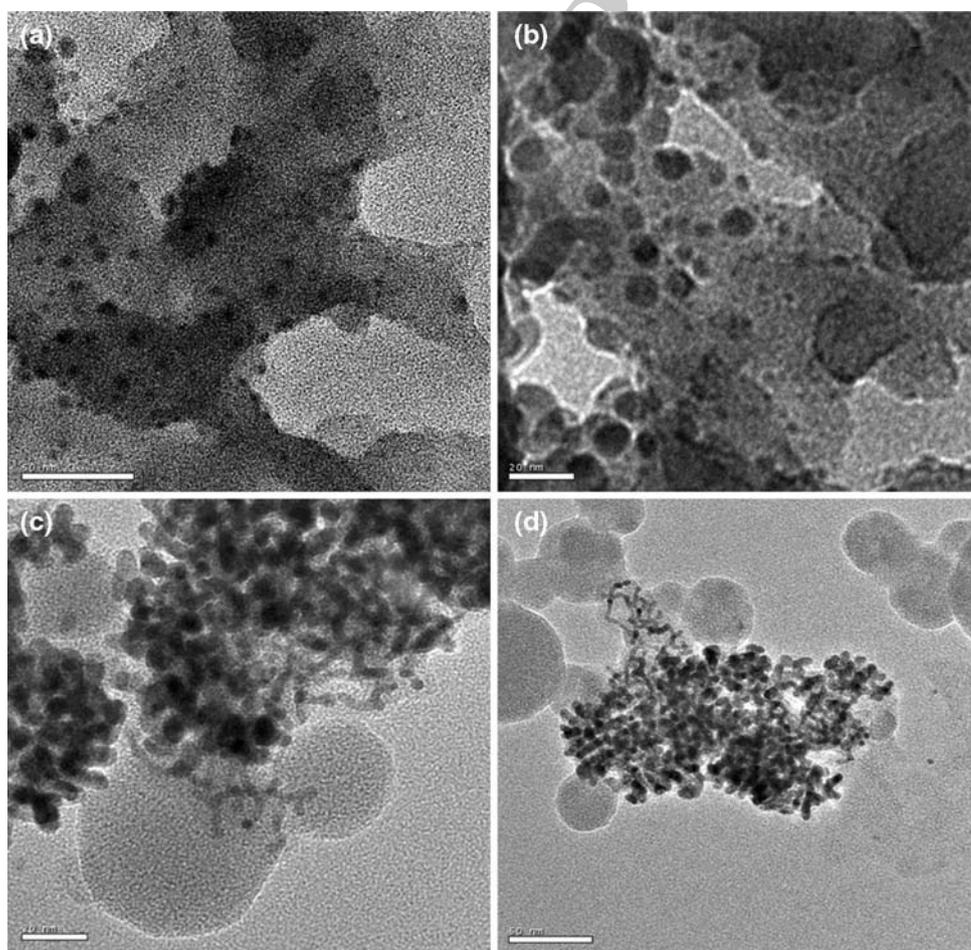


Fig. 6 TEM images of (a) & (b) Ag-PANI-PMO₁₂ and (c) & (d) Au-PANI-PMO₁₂



271 clear crystalline planes aligned along a specific direction
 272 with a d spacing of 2.36 Å. Figure 8b indicated the dark
 273 Au nanorod arms surrounded by a grayish sheath of PANi
 274 in the Au-PANi-PMO₁₂ composite. The planes of the rods

are aligned with a d spacing of 2.38 Å. The electrical
 conductivities of the Ag-PANi-PMO₁₂ and Au-PANi-PMO₁₂
 composites measured with a four-probe technique were
 found to be 12.5 and 6.5 S cm⁻¹, respectively.

275
 276
 277
 278

Fig. 7 Particle size distribution of (a) Ag-PANI-PMo₁₂ and (b) Au-PANI-PMo₁₂

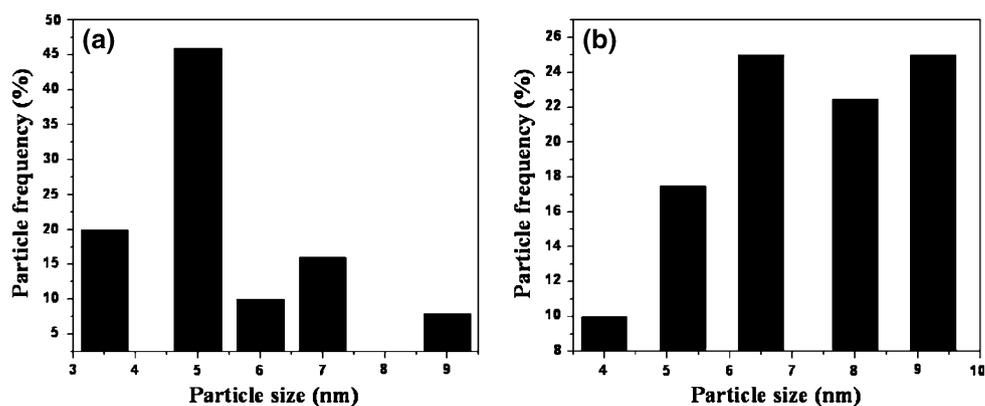
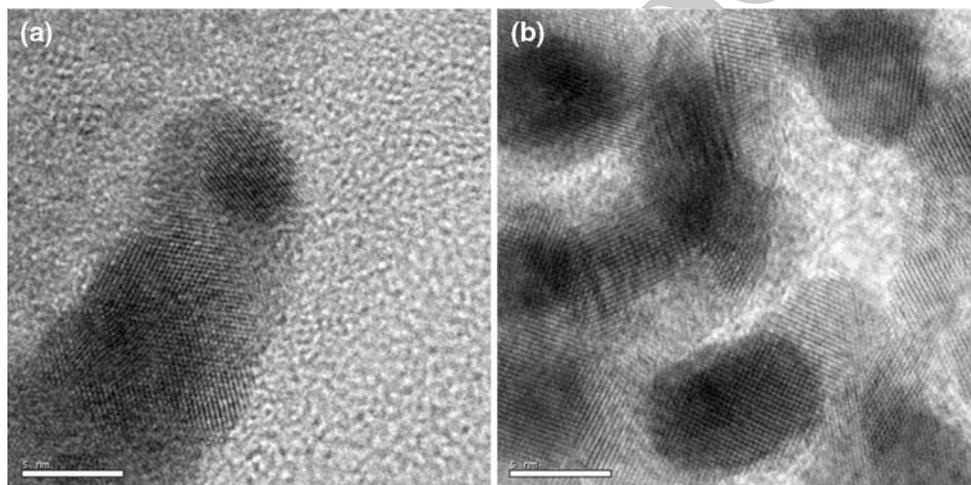


Fig. 8 HRTEM images of (a) Ag-PANI-PMo₁₂ and (b) Au-PANI-PMo₁₂



279 Conclusions

280 In conclusion, a simple method has been introduced to
 281 prepare Ag and Au nanoparticle containing organic–inor-
 282 ganic nanocomposites of PANi and PMo₁₂ using the
 283 excellent electron transfer capability of polyoxometalates.
 284 PMo₁₂ has served dual role in the formation of the
 285 nanocomposites; it served as oxidizing agent for the
 286 polymerization of aniline and reducing agent for the for-
 287 mation of metal nanoparticles. In particular, the
 288 synthesized nanocomposites exhibited embedded metal
 289 nanoparticles in the polymer matrix. Furthermore, the
 290 method can be extended to the synthesis of other con-
 291 ducting polymers and opens up a new route to prepare
 292 inorganic–organic nanocomposites with wide variation of
 293 properties. It should also stimulate the exploration of
 294 applications of these nanocomposites especially in fields
 295 such as sensors, catalysis, and composite materials.

296 References

- 297 1. R. Gangopadhyay, A. De, Chem. Mater. **12**, 608 (2000)
 298 2. Z. Peng, L. Guo, Z. Zhang, B. Tesche, T. Wilke, D. Ogermann, S.
 299 Hu, K. Kleinermanns, Langmuir **22**, 10915 (2006)
3. Y. Xian, Y. Hu, F. Liu, Y. Xian, H. Wang, L. Jin, Biosens. Bioelectron. **21**, 1996 (2006)
4. A.A. Athawale, S.V. Bhagawat, P.P. Katre, Sens. Actuators, B Chem. **114**, 263 (2006)
5. W.U. Huynh, J.J. Dittmer, A.P. Alivisatos, Science **295**, 2425 (2002)
6. R.J. Tseng, J. Huang, J. Ouyang, R.B. Kaner, Y. Yang, Nano. Lett. **5**, 1077 (2005)
7. M.A. Malik, M.T. Galkowski, H. Bala, B. Grzybowska, P.J. Kulesza, Electrochim. Acta. **44**, 2157 (1999)
8. C.C. Hu, E. Chen, J.Y. Lin, Electrochim. Acta. **47**, 2741 (2002)
9. T. Amaya, D. Saio, T. Hirao, Tetrahedron Lett. **48**, 2729 (2007)
10. B. Rajesh, P. Zelenay, Nature **443**, 63 (2006)
11. B. Rajesh, K.R. Thampi, J.M. Bonard, A.J.M. Evoy, N. Xanthopoulos, H.J. Mathieu, B. Viswanathan, J. Power Sources **133**, 155 (2004)
12. B. Rajesh, K.R. Thampi, J.M. Bonard, H.J. Mathieu, N. Xanthopoulos, B. Viswanathan, J. Power Sources **141**, 35 (2005)
13. E. Granot, E. Katz, B. Basnar, I. Willner, Chem. Mater. **17**, 4600 (2005)
14. S. Tian, J. Liu, T. Zhu, W. Knoll, Chem. Mater. **16**, 4103 (2004)
15. A.A. Mikhaylova, E.B. Molodkina, O.A. Khazova, V.S. Bagozky, J. Electroanal. Chem. **509**, 119 (2001)
16. S.M. Marinakos, D.A. Shultz, D.L. Feldheim, Adv. Mater. **11**, 34 (1999)
17. A. Marc, G.Y. Breimer, S. Sheldon, A.S. Omowunmi, Nano Lett. **1**, 305 (2001)
18. H.H. Zhou, X.H. Ning, S.L. Li, J.H. Chen, Y.F. Kuang, Thin Solid Films **510**, 164 (2006)

- 330 19. D.W. Hatchett, M. Josowicz, J. Janata, Chem. Mater. **11**, 2989
331 (1999) 347
- 332 20. S.T. Selvan, J.P. Spatz, H.A. Klok, Adv. Mater. **10**, 132 (1998) 348
- 333 21. M.M. Oliveira, E.G. Castro, C.D. Canestraro, D. Zanchet, D.
334 Ugarte, L.S. Roman, A.J.G. Zarbin, J. Phys. Chem. B. **110**, 17063
335 (2006) 349
- 336 22. A. Chen, H. Wang, X. Li, Chem. Commun. 1863 (2005) 350
- 337 23. T.S. Sarma, D. Chowdhury, A. Paul, A. Chattopadhyay, Chem
338 Commun. 1048 (2002) 351
- 339 24. E. Papaconstantinou, Chem. Soc. Rev. **18**, 1 (1989) 352
- 340 25. G. Bidan, M. Lapkowski, J.P. Travers, Synth. Metals **28**, C113
341 (1989) 353
- 342 26. P.G. Romero, N.C. Pastor, M.L. Cantu, Solid State Ionics
343 **101–103**, 875 (1997) 354
- 344 27. M.L. Cantu, P.G. Romero, Chem. Mater. **10**, 698 (1998) 355
- 345 28. J. Vaillant, M.L. Cantu, K.C. Gallegos, N.C. Pastor, P.G.
346 Romero, Prog. Solid State. Chem. **34**, 147 (2006) 356
29. L. Adamczyk, P.J. Kulesza, K. Miecznikowski, B. Palys,
M. Chojak, D. Krawczyk, J. Electrochem. Soc. **152**, E98 (2005) 357
30. L.J. Van der Pauw, Philips Res. Rep. **13**, 1 (1958) 358
31. A. Troupis, A. Hiskia, E. Papaconstantinou, Angew. Chem. Int.
Ed. **41**, 1911 (2002) 359
32. E. Papaconstantinou, J. Chem. Soc. Faraday Trans. **78**, 2769
(1982) 360
33. I.A. Weinstock, Chem. Rev. **98**, 113 (1998) 361
34. A. Muller, S.Q.N. Shah, H.B.M. Schmidtman, Nature **397**, 48
(1999) 362
35. V. Kogan, Z. Aizenshtat, R.P. Biro, R. Neumann, Org. Lett. **4**,
3529 (2002) 363
36. A.V. Gordeev, B.G. Ershov, High Energ. Chem. **33**, 218 (1999) 364
37. S. Mandal, A.B. Mandale, M. Sastry, J. Mater. Chem. **14**, 2868
(2004)
38. M. Verga, E. Papaconstantinou, M.T. Pope, Inorg. Chem. **9**, 662
(1970)

UNCORRECTED PROOF